# TEM characterization and high-resolution modelling of second-phase particles of V and Ti containing TWIP steel under uniaxial hot-tensile condition

A.E. Salas-Reyes[a,b], I. Mejía[a*], A. Ruíz-Baltazar[c], J.M. Cabrera[d]

[a] Instituto de Investigación en Metalurgia y Materiales, Universidad Michoacana de San Nicolás de Hidalgo, Edificio "U-3", Ciudad Universitaria, Morelia 58030, Michoacán, México.

[b] Departamento de Ingeniería Metalúrgica, Facultad de Química, UNAM. Ciudad Universitaria. Ciudad de México, 04510, México.

[c] CONACYT - Centro de Física Aplicada y Tecnología Avanzada, UNAM, Boulevard Juriquilla 3001, Santiago de Querétaro, Qro. 76230, México.

[d] Departament de Ciència dels Materials i Enginyeria Metal·lúrgica, EEBE–Universitat Politècnica de Catalunya, c/ Eduard Maristany 10-14, Barcelona 08019, Spain.

## Abstract

The composition and crystallographic nature of precipitates in microalloyed advanced high-strength steels (AHSS) greatly influence their microstructure evolution and mechanical behavior. Second-phase precipitation in a high-Mn austenitic TWIP steel single microalloyed with V and Ti under uniaxial hot-tensile condition was experimentally and theoretically studied using high-resolution TEM (HRTEM) images. For this purpose, TEM carbon replica technique, image treatment, and computer simulation were used to determine crystallographic

* Corresponding author. Fax: +52 443 322 3500 x 4009. E-mail addresses: imejia@umich.mx, i.mejia.granados@gmail.com (I. Mejía).

features of particles and compared with experimental measurements. Results revealed particle morphologies depending on their crystallographic orientation, namely hexagonal-type for TWIP-V steel and rectangular-type in the case of TWIP-Ti steel. Measurements on particle size ranged 10 to 190 nm in both steels. HRTEM digital image processing allowed correcting obtained FFT diffraction patterns, where interplanar distance measurements indicate the presence of VC and TiC compounds. In the case of the modeled particles, it was possible the identification of the NaCl-type crystal structure, which in turns correctly related with experimental morphologies. Finally, theoretical simulations based on the multislice approach of the dynamical theory of electron diffraction allowed modeling HRTEM images. Thus, results indicate that current characterization and simulation procedure is helpful in recognizing the crystallographic nature of second-phase particles formed in the studied TWIP steels.

**Keywords:** High-Mn TWIP steel; V and Ti microalloying elements; Uniaxial hot-tensile test; HRTEM simulation; Second-phase particles.

## 1. Introduction

Lately, as the automotive industry develops due to environmental and safety requirements around the world, particular interest has been focused in high-Mn Twinning Induced Plasticity (TWIP) steels. These TWIP steels have gained considerable interest because their superior mechanical properties in terms of strength, ductility and energy absorption. This combination of outstanding mechanical properties is governed by the deformation mechanism, which is controlled by mechanical twinning and it is associated to the low stacking fault energy (SFE).[1] Mechanical twins interfere with the glide of dislocations like ordinary grain boundaries, causing the reduction of the mean free path of dislocations, enhancing work hardening, i.e., promoting a dynamic Hall-Petch effect.[2] Extensive research work has been

carried out on high-Mn TWIP steels employing different compositions as an attempt to improve both cold and hot mechanical behavior. However, under conventional industrial processing routes, TWIP steels display a persistent low yield stress. The microalloying concept is an ideal way for improving this problem without degrading deformation capability. The major roles of microalloying elements include the control of grain coarsening by pinning the grain boundaries, solid solution and precipitation strengthening, and the increase in hardenability. On the basis of thermodynamics and kinetics considerations, stable carbides, nitrides and carbonitrides (precipitated at high temperatures) in microalloyed TWIP steels have been known to occur at various stages during and after solidification, thermal and thermo-mechanical processing.[3-6] Due to the small size of second-phase particles (typically few tenths of nanometers), conventional transmission electron microscopy (TEM), appears as one of the most widely used techniques for their characterization and size measurement.[7] Broadly, thin foils and carbon extraction replicas TEM techniques are extensively used for the quantitative measurements of shape, size, crystallography and distribution of precipitates, covering relatively large areas for punctual analysis. Of particular importance in high-Mn austenitic TWIP steels is the role of microalloying elements in forming TiC, NbC and VC particles. It has been determined that these carbides form a NaCl (B1) crystal structure, which is described as cubic-F with a motif consisting of a metal atom located at    and a carbon atom at $\left(0,0,\frac{1}{2}\right)$.[8] The reported lattice parameters are 4.32 Å for TiC, 4.47 Å for NbC and 4.17 Å for VC at room temperature.[9] Lately, Bobynko et al.[10] studied the structure and chemistry of V and Nb nanoprecipitates in two Fe-20Mn-0.6C-1.5Al high-Mn steels containing 0.3 wt% V and 0.1 wt% Nb, respectively, under controlled heat treatment between 850 and 950 °C followed by a hot deformation schedule. In particular, they found that nucleation of VC and NbC precipitates often occurs at pre-existing TiC particles as impurities in the bulk steel. On

3

one hand, the Ti/V ratios would probably lead to slight variations in VC lattice parameter from 4.16 up to 4.2 Å. On the other hand, the measured NbC lattice parameter was 4.41 Å. Based on this study, they concluded that Dual Electron Energy Loss Spectroscopy (DualEELS) allows absolute quantification of nanoscale precipitates in steels in terms of the contribution of single elements in the thicknesses of each precipitated particles by means of an edge intensity maps treatment image procedure. However, the most interesting contribution of these authors is found elsewhere [11], where a meticulous and refined procedure was stablished as an effort on extracting spectrum images digitally for quantitative analysis of precipitates chemistry throughout exploiting the benefits provided by DualEELS spectrum acquisition. They studied two high-Mn steels with the same base alloy containing 0.2 wt% of V and 0.1 wt% of Nb. Both steels had a similar experimental processing schedule consisting of hot rolling, solution heat treatment, hot compression deformation and fast cooling. In summary, after image corrections a scaled matrix spectrum was obtained. Thanks to this procedure, V and Nb precipitation maps and chemical profiles were obtained. Furthermore, DualEELS spectrum images acquired around buried nanoscale precipitates can be treated in such a way that precipitates signal allow distinguishing them from other matrix contributions, such as carbon contamination. So, this procedure could be considered as a digital version of the well-known extraction replica.

Recently, Llanos et al.[5] investigated the effect of V content (0.1 and 0.2 wt%) in high-Mn austenitic steels (20, 30 wt% of Mn and 0.2, 0.6, 1 wt% of C) in terms of thermally activated processes and softening kinetics. For this purpose, double-hit torsion tests from 700 to 1100 °C at a constant strain rate of 1 s$^{-1}$ were carried out. The precipitation state was examined using TEM through carbon replicas. Their results indicate that strain-induced precipitation is sluggish and it mainly occurs for the 20Mn-0.6C-0.2V or 30Mn-1C-0.1V chemical combinations, leading to large retardation of softening kinetics. On the other hand,

strain-induced precipitation is suppressed reducing carbon content, independent on N level. Furthermore, abundant precipitation with particle size ranging from 5 to 25 nm was detected in samples tested between 850 and 900 °C. Evidently, particle size increases as temperature does. A major conclusion concerns to the softening kinetics because the complex interaction between recovery and recrystallization when strain-induced precipitation takes place.

Even though the scientific work on the hot deformation behavior of TWIP steels has increased lately and many researchers have characterized second-phase particles through TEM using both thin foil and carbon extraction replica techniques, there is still scarce information concerning the crystallographic nature of precipitates in high-Mn TWIP steels. Therefore, it is an important issue for scientific knowledge and steel industry to have a better understanding on chemistry and crystallographic of second-phase particles formed at higher temperatures in high-Mn austenitic TWIP steels. Thereby, the aim of this research work is to study the essential crystallographic features of V and Ti precipitated particles in a Fe-Mn-C-Al-Si austenitic TWIP steel after uniaxial hot tensile test by using simultaneous high-resolution TEM (HRTEM) characterization and simulation.

## 2. Experimental Section

Two experimental single V and Ti microalloyed high-Mn austenitic TWIP steels were prepared by induction melting employing high-purity raw materials. Their chemical compositions are given in **Table 1**. Detailed information about fabrication process, sample preparation and hot-tensile testing can be found elsewhere.[4] Thermodynamic phase equilibria predictions were performed using FactSage® thermochemical software[12] together with the FSstel calculation module that enable pure substances and solution compounds databases,[13] described into a sub-lattice model with carbon, nitrogen and vacancies on interstitial sites. In order to fully predict chemical species and transition temperatures, calculations were carried out every 10 °C in the temperature range between 600 and 1600 °C.

**Table 1.** Chemical composition of studied TWIP steels (wt%).

| TWIP steel | Mn | C | Si | Al | Ti | V | N | Fe |
|---|---|---|---|---|---|---|---|---|
| TW-V | 21.2 | 0.56 | 1.3 | 1.46 | - | 0.11 | 0.0120 | Bal. |
| TW-Ti | 22.2 | 0.57 | 1.2 | 1.8 | 0.0216 | - | 0.0120 | Bal. |

After fracture, samples tested in the temperature range of 800-900 °C were collected, longitudinally sectioned close to fracture tip and prepared metallographically to obtain carbon extraction replicas for conventional TEM examination. Samples surface were etched using 5% Nital solution during 20 s to dissolve metallic matrix. Immediately, vacuum carbon deposition was done during 8.5 s. Operational conditions were as follows: i) Vacuum at 50 militors, ii) Current at 50 Amperes, and iii) Electrode dimensions of 1 mm in diameter and 4 mm in length. Then, samples were etched again with 10% Nital solution during 12 s to remove the particles from the matrix. Finally, carbon film was detached in distilled water and collected in 3 mm copper grid. TEM characterization was perform in a FEI Tecnai F20 transmission electron microscope operating at 200 keV under bright field mode for analyzing the chemical composition, distribution and size of precipitated particles. On the other hand, HRTEM images were digitally processed and simulated through SimulaTEM software using the multilayer method. First, the experimental HRTEM images were corrected using modern filters such as Gaussian blur, which generates more legible images. Then, based on the corrected Fast Fourier Transform (FFT) diffraction pattern, better accurate interplanar measurements were done. So, in order to develop the models in SimulaTEM software, the following simulation parameters were used: i) 200 keV, ii) -15.8364 Å of defocus, iii) 12 Å of defocus spread and iv) 1 milliradian of beam spread. Finally, theoretical simulations based on the multislice approach of the dynamical theory of electron diffraction were carried out to generate HRTEM images.[14]

6

## 3. Results and Discussion

### 3.1 Thermodynamic Predictions

The equilibrium phase behavior calculated using FactSage® for the current TWIP steels is shown in **Figure 1**.
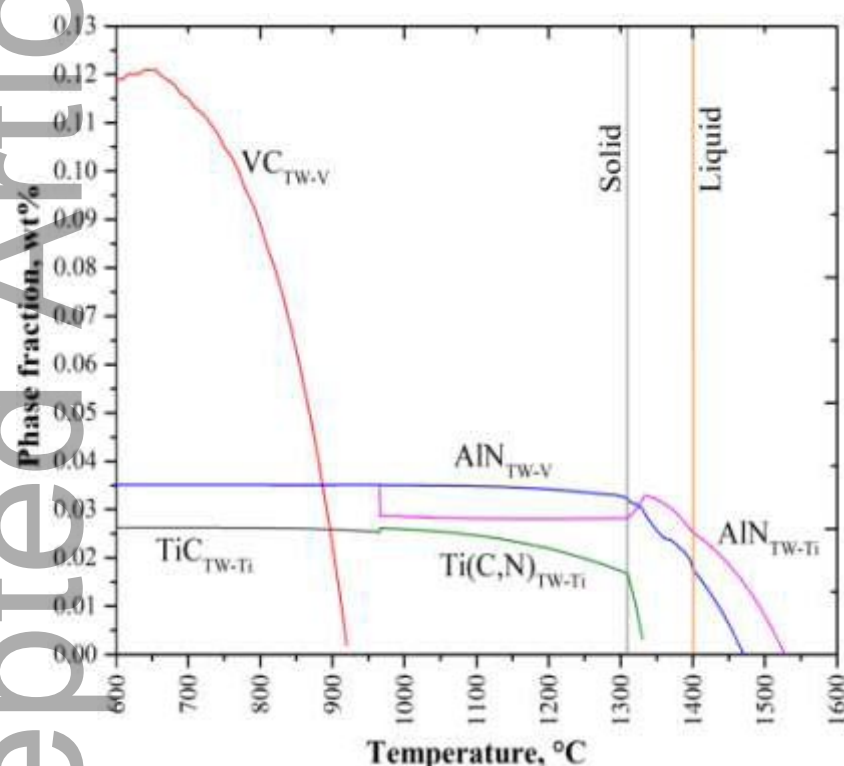


**Figure 1.** Phase transformation behavior and equilibrium compounds of single V and Ti microalloyed TWIP steels predicted by FactSage®.

It can be seen that solidus and liquidus transition temperatures are situated at 1313 and 1400 °C, respectively, in both steels. In the case of V-containing TWIP steel (TW-V), precipitation of VC particles takes place in solid state at 920 °C because there is enough carbon available for its precipitation. This second-phase reaches a maximum value in a weight fraction of 0.01210 at 654.7 °C and then begins to decrease as temperature decreases. Baker

7

[15] reported that the solubility of VC in austenite for low alloyed carbon steels is significantly higher than in other microalloyed steels. It is worth noting that VN do not form since there is no N left in solid solution after AlN formation. On the other hand, in the case of the Ti-containing TWIP steel (TW-Ti), precipitation of second-phase Ti(C,N) particles begins in the solid-liquid zone at 1333.7 °C. Based on this information, it is clear that dissolved N in molten steel is stabilized by Ti addition.

It is worth noting a variation of Al content in these high-Mn alloys, related to the AlN precipitation starting temperature. In the case of the TW-V steel, AlN precipitation occurs at 1470 °C, and in the TW-Ti steel, this precipitation takes place at 1530 °C. Because N has high chemical affinity to both Al and Ti, the susceptibility to form AlN or Ti(C,N) particles is well established for the TW-Ti steel phases prediction. Ti(C,N) precipitation forms at 1333.7 °C, temperature in which AlN precipitation is suppressed by Ti(C,N) evolution as temperature decreases, because TiN requires some of the N forming AlN at higher temperatures. Furthermore, it is observed that Ti(C,N) starts forming during the early stages of solidification. However, at 965.4 °C thermodynamic conditions are only favorable in forming AlN in a constant weight fraction value of 0.03512, as AlN does in the case of the TW-V steel, where TiC precipitation is now the stable phase taking place until the lowest studied temperature with a weight fraction value of approximately 0.02627.

In summary, as uniaxial hot-tensile tests were carried out at an intermediate temperature range, the expected fraction of precipitated second-phase particles are 0.0230 wt% for VC at 900 °C in the TW-V steel and 0.0262 wt% for TiC at 800 °C in the TW-Ti steel.

## 3.2 Morphological Analysis

TEM observations of precipitates obtained through carbon extraction replicas of single V and Ti microalloyed TWIP steel are presented in **Figure 2**a-b. Additionally, in order to identify

8

the chemical composition of these particles, an Energy Dispersive Spectroscopy (EDS) spectrum was taken from the particles identified with a red "X" mark into micrographs and the obtained diffractograms are shown in **Figure 2**c-d.
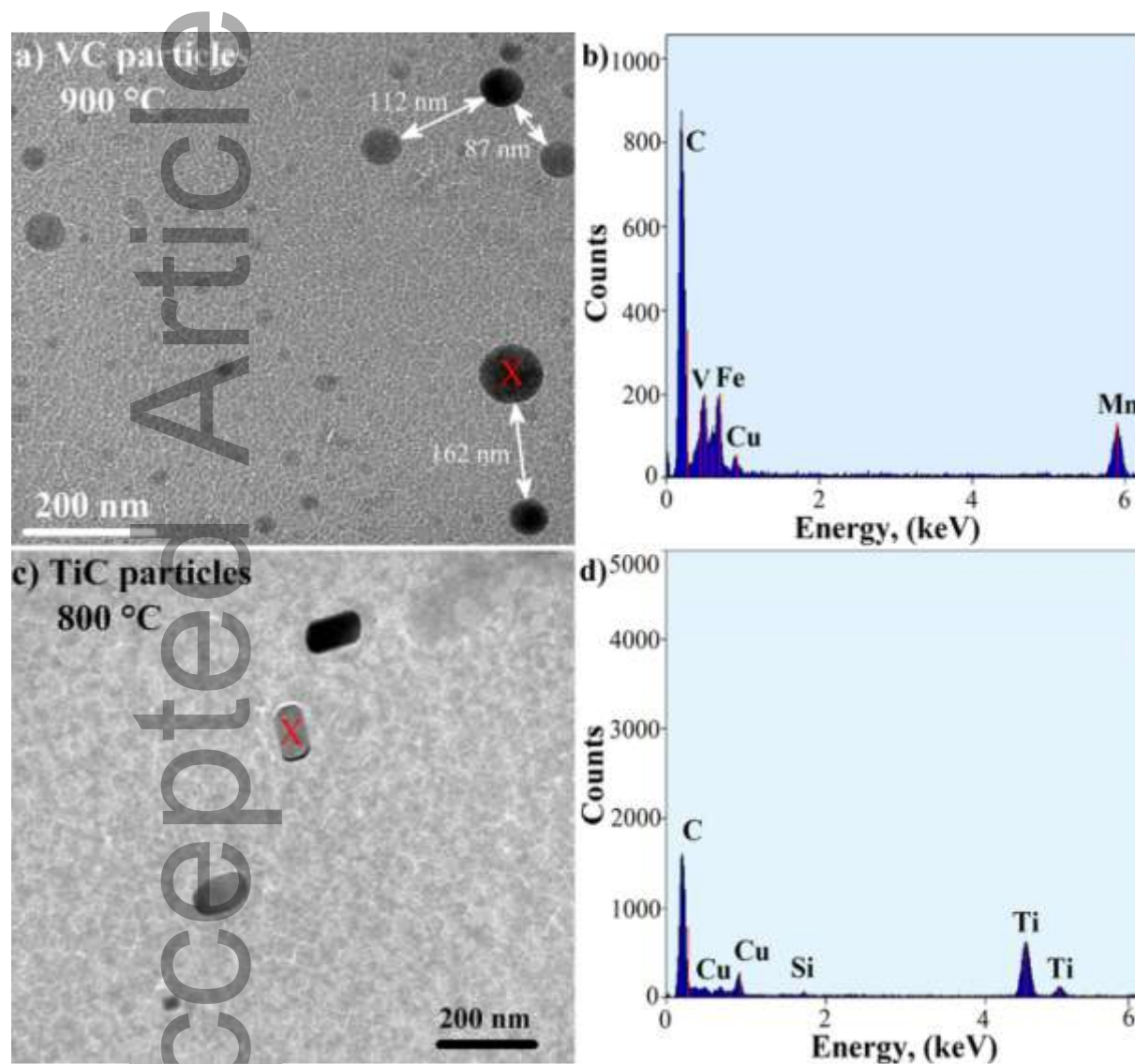


**Figure 2.** Low magnification TEM bright field images of second-phase particles and their EDX chemical analysis for: a-b) V-containing TWIP steel and c-d) Ti-containing TWIP steel.

Spectrum analysis clearly indicates the presence of both types of carbides, VC and TiC, respectively. It is important to consider the effect of carbon content related to the carbon film of sample during elemental data acquisition. Furthermore, in the case of TW-V steel, it can be

9

observed that VC precipitation is basically coherent within the austenitic matrix and these particles apparently seem to have rounded-type morphology, as microscope magnification displays to the reader. On the other hand, in the case of TW-Ti, TEM observations revealed that most TiC precipitates have faceted shape morphologies, e.g. cuboids or enlarge plates (rectangular-type morphology) are easily noticeable. Ti element is characterized by its low solubility in austenite, and a small Ti addition can result in a strong carbides/carbonitrides precipitation in TWIP steel. It should be noted that there is a preferential line arrangement of precipitates, which indicates precipitation at austenitic grain boundaries, as it has been reported by present authors.[4] As shown in the thermodynamic analysis, V and Ti microalloying elements in TWIP steel can precipitate out at lower temperatures. Particle statistical analysis carried out on TEM bright field micrographs is presented in **Figure 3**. In the case of V-rich carbides, it indicates that particle sizes range from 10 to 190 nm, with an average particle size of 38 nm. It is worth noticing the large amount of V carbides with average modal sizes of 10, 30 and 70 nm.

Additionally, it is important to remark that the largest particles are surrounded generally by other small particles, with a separation distance among them ranging 67 to 356 nm and there are particular cases where observed separation corresponds to approximately 12 nm. On the other hand, the average particle size for TiC particles is about 40 nm, while the largest one is about 135 nm, and the smallest one is approximately 10 nm.
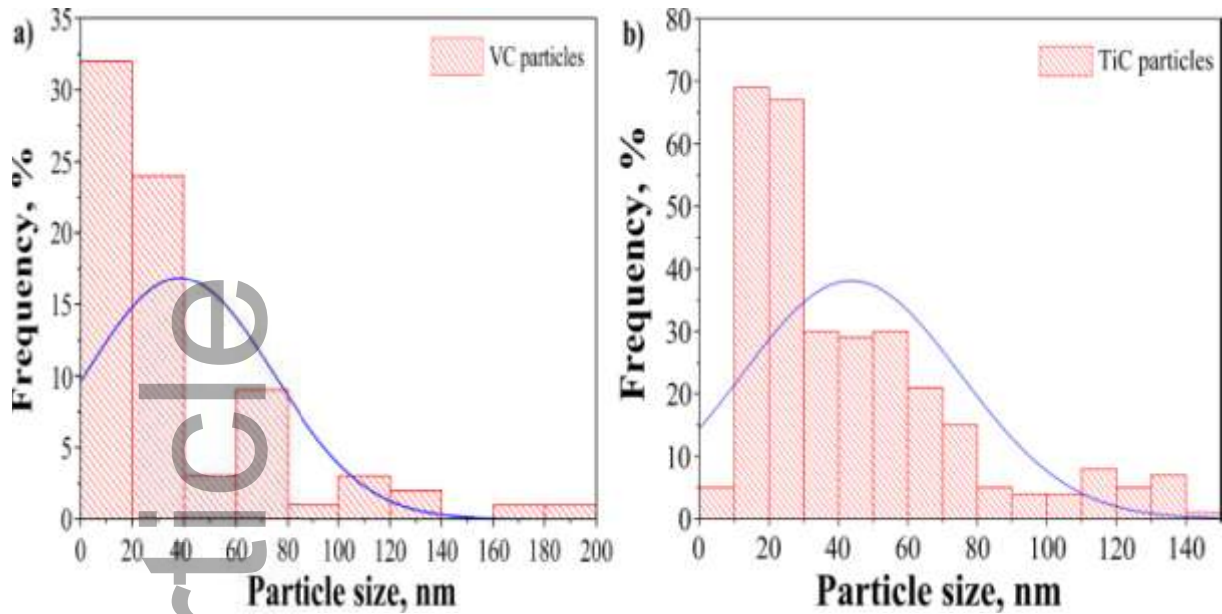
**Figure 3.** Particle size distribution: a) TW-V steel hot-tensile tested at 900 °C and b) TW-Ti steel hot-tensile tested at 800 °C.

## 3.3 Crystallographic interpretation

By selected area diffraction patterns, HRTEM images were obtained and processed as a first attempt in characterizing these V and Ti-rich carbide particles. However, the effect of carbon content related to the carbon film of replica samples during elemental data acquisition is an important issue to be considered when chemical analysis of compounds is performed. Hence, with the aim to know in depth carbide type-compound, HRTEM image processed through the Fast Fourier Transform (FFT) method (see **Figure 4**a-b) has allowed correlated already known stoichiometry values of V-rich carbides with current experimental VC compound, as indicated by the interplanar measurements carried out on a Moiré fringe contrasted spacing image, which has been inserted in image **Figure 4**b for a better visualization. In accordance, a lattice parameter of 4.174 Å in the [220] zone axis was obtained according to PDF# 96-900-8765 [16] and compared with the lattice parameter of 4.173 Å, reported by Villars.[17] This identified data corresponds with a structure exhibiting the cubic crystal system, related to the

11

space group Fm-3m (225). The variation in lattice parameter in the present work with the above mentioned ones, refers to the experimental procedure limitations in obtaining more clearly HRTEM images from the bulk particles, because periphery thickness and carbon film overshadow effect is also expected to occur. In general terms, Moiré fringe contrast can be used as a high resolution imaging method to investigate the properties of small precipitates (e.g. lattice parameters).[21]
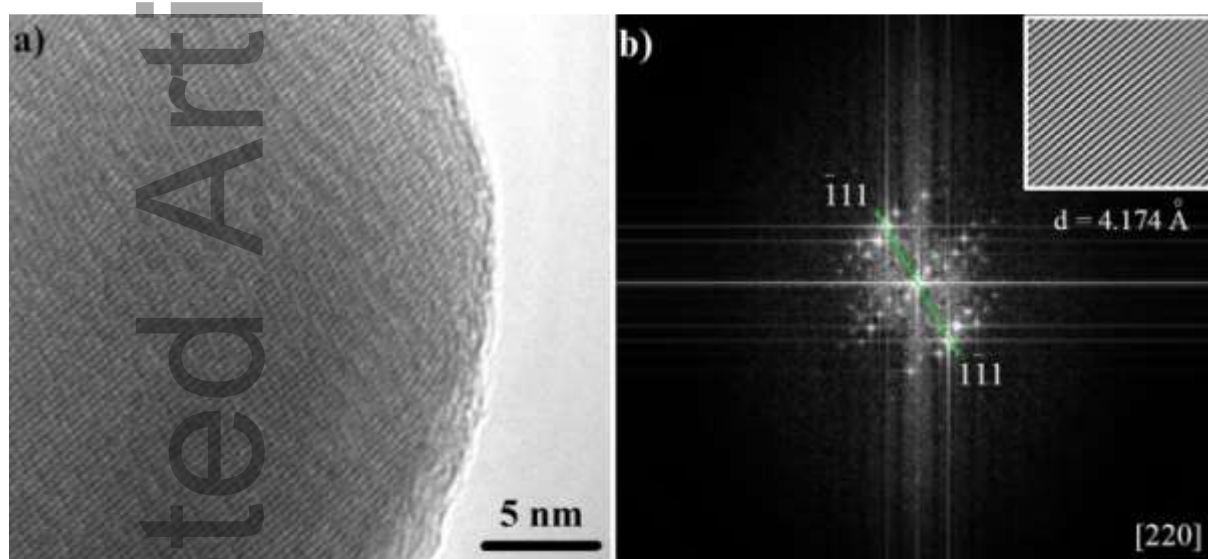


**Figure 4.** V-rich carbide in TW-V: a) High-resolution TEM image and b) Indexed compound orientation according to the FFT.

In the case of **Figure 5**a, HRTEM image treatment indicates interplanar distances of 0.470 and 0.210 nm, associated with $\left(2\bar{2}0\right)$ and $\left(\bar{1}\bar{1}1\right)$ planes. These measurements have confirmed the presence of the VC compound. In **Figure 5**b, Fast Fourier Transform (FFT) diffractogram obtained from the HRTEM in the $[220]$ axis zone of the VC is presented. The intensities associated with planes $\left(2\bar{2}0\right)$ and $\left(\bar{1}\bar{1}\bar{1}\right)$ are also observed. Thus, the presence of the cubic structure of the VC was confirmed. Yen et al.[18] reported a NaCl-type crystal structure for

12

vanadium carbides in V-containing TWIP steel, which obeys the cube-on-cube orientation relationship (OR), reporting values of 0.359 nm for austenite and 0.415 nm for vanadium carbide.
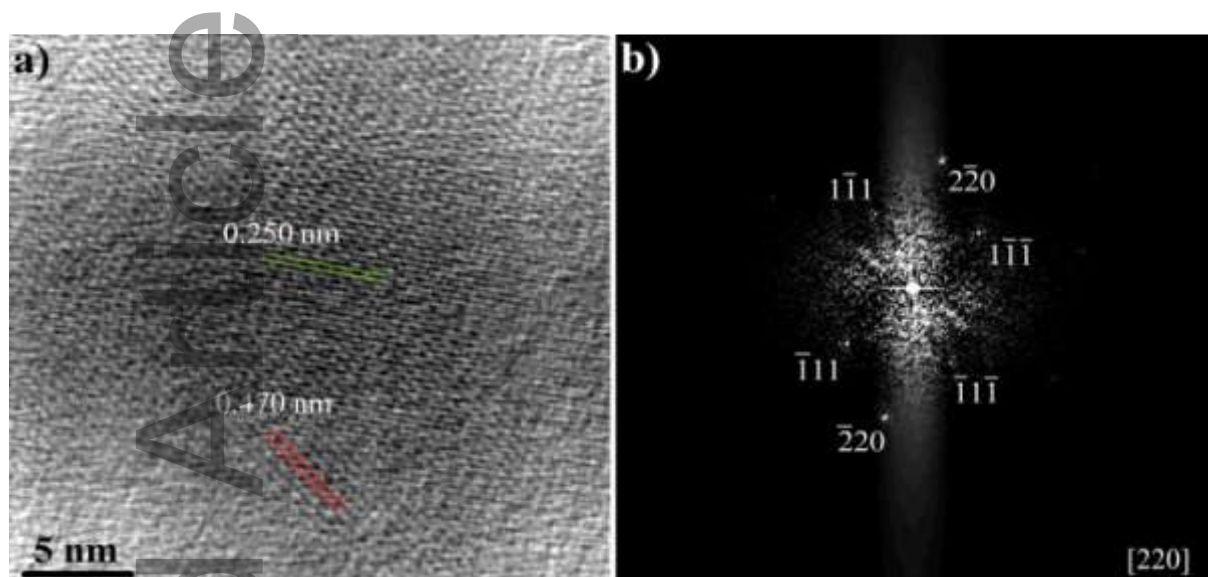


**Figure 5.** V-rich carbide in TW-V: a) Experimental high-resolution TEM image and b) Fast Fourier Transform (FFT) electron diffractogram.

Since V is a stronger carbide former, it has been reported that the lattice parameters of the B1 (Fm3m) NaCl -type compounds of V are 0.41285 nm for $VC_{0.75}$ to 0.41686 nm for $VC_{0.92}$.[19] In contrast, ideal stoichiometry is not generally found in the ordered phases. In the present work, thermodynamic calculations indicates that VC should be completely dissolved in austenite up to 900 °C, but at lower temperatures a problem with its solubility product is evidenced in terms of the compound stoichiometry relationship. The perceived differences in stoichiometry differ from author to author, where the most undertaken stoichiometry historically reported has been $V_4C_3$[20-23] instead of VC[24,25] but no unambiguous diffraction experiments have been well-documented for the system Fe-V-C containing $V_4C_3$ compound.[7]

13

In the same manner, **Figure 6**a shows the experimental HRTEM image acquired for the Ti-rich carbide. Measurements carried out on the interplanar spacing indicated the existence of TiC compound when compared with crystallographic card number PDF 6-614.[26] Corresponding values of 0.242 and 0.2109 nm are associated to $(1 1 1)$ and $(2 0 0)$ planes,[27] respectively. The well-stablished intensities in planes $(1 1 1)$ and $(2 0 0)$ in the Fast Fourier Transform (FFT) electron diffractogram in the analyzed HRTEM image are in agreement with the $[\bar{2} 0 \bar{2}]$ zone axis (see **Figure 5**b). NaCl-type structure of TiC compounds was determined by von Schwarz and Summa,[28] which exhibits the space group Fm3m (225) cubic structure.
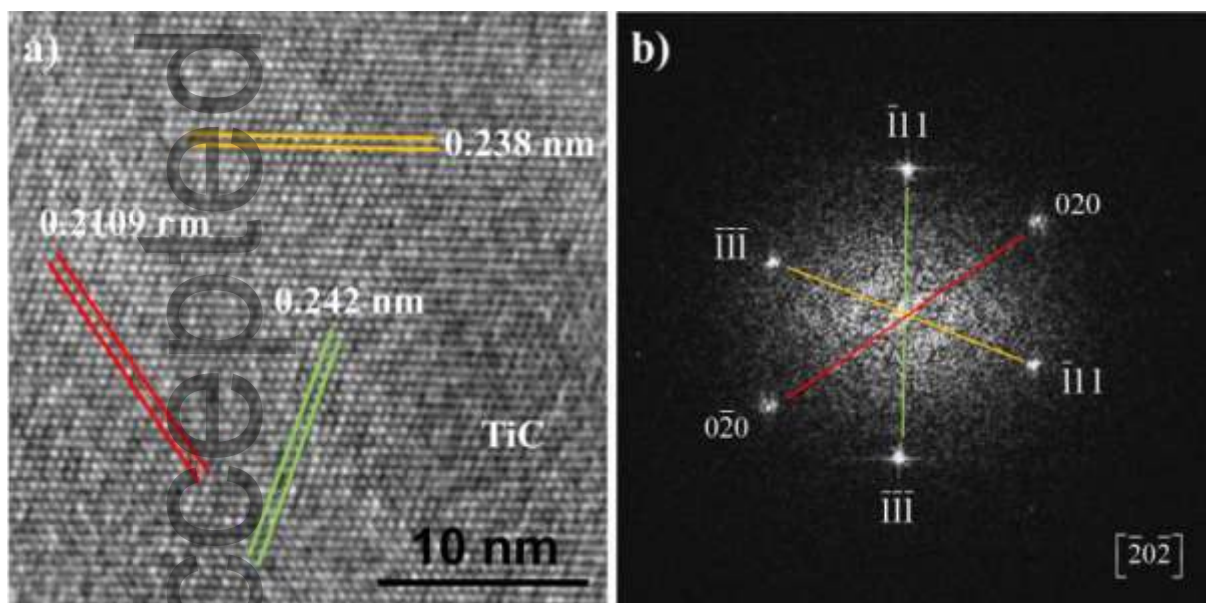


**Figure 6**. Ti-rich carbide in TW-Ti: a) Experimental high-resolution TEM image and b) Fast Fourier Transformation (FFT) electron diffractogram.

Lv and Gao [29] pointed out that carbon concentration clearly influences the atomic structure of titanium carbides, indicating that there are three major TiC crystal types, hexagonal, coexistence of hexagonal and cubic, and cubic, that dominates the titanium carbide structure

14

for different carbon concentrations. Also, it is well-known that titanium carbide is a refractory compound that has a wide range of stoichiometry homogeneity (i.e. $TiC_{0.6} - TiC_{0.98}$).[30] Particularly, it has been stated that in supersaturated austenitic solid solution, TiC carbides adopt a cube to cube OR with respect to the austenitic matrix.[31] Alternatively, it is worth noting that a simulated PDE is determinant in indexing the computer-generated HRTEM diffraction spectra showed above in **Figure 5** and **6**.

Accordingly to this, both VC and TiC superlattice, modeled through the use of SimulaTEM and Carine Crystal software, have indicated that when the NaCl unit cell rotates on its symmetrical axes (see **Figure 7**a), typically VC and TiC particles morphologies, as observed experimentally, are clearly evident. So, based on crystal orientation, several geometric configurations can be perceived: hexagonal, round and rectangular-type morphologies. Thus, if the preferential orientation $[111]$ is defined when crystal rotates, the cubic structure of the VC can be completely observed as hexagonal-type morphology. Therefore, it can be stated that the VC crystal structure can be fully identified on the austenitic matrix throughout computational approach.

However, it is observed that the main morphology of TiC varies slightly in shape, from a regular to non-uniform rectangle-type morphology, when the rotation axis $[220]$ of the crystal is altered in accordance with the plane $(100)$, as it can be perceived in **Figure 2**c, a slightly distorted incrustation of TiC particles can be observed at approximately 10º. This behavior generates well-defined non-uniform rectangle-type morphology, which apparently coarse or wide central corners of the single cubic crystal. The fact in having these two morphologies at the same time can be attributed to the effect of imposed stress in redistributing plastic deformation, as mentioned in the experimental section, which in turns slightly modifies TiC incrustation or pinning orientation at grain boundaries, as austenitic

15

grains deform too. Consequently, there is a great correlation between simulated and experimental particle chemistry, crystallographic and thermodynamic predictions of studied TWIP steels.

Taking into account the above mentioned, simulated HRTEM diffraction spectra and experimental ones, have a great similarity, as shown **Figure 7**. In this way, it can be demonstrated that the proposed modeling procedure is adequate in characterizing V and Ti-rich carbides through carbon extraction replicas.
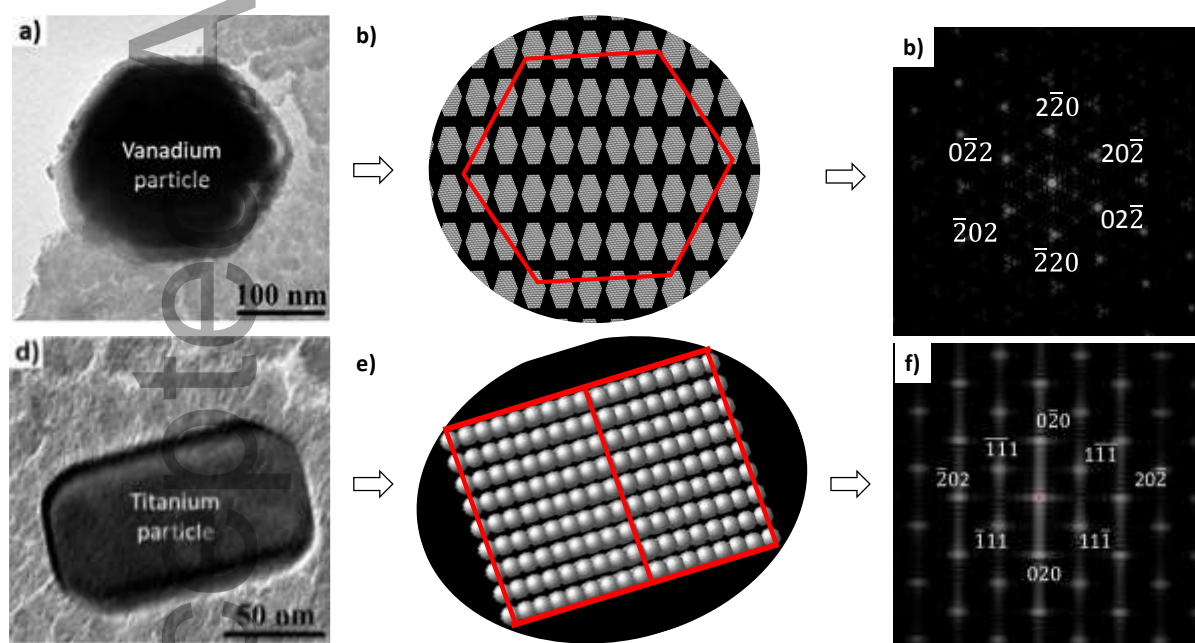


**Figure 7.** Experimental particle morphology, modeled superlattice structure and simulated HRTEM diffraction spectra.

## 4. Conclusions

Series of precipitation characterization in carbon extraction replica samples in TWIP steels single microalloyed with V and Ti were carried out using HRTEM images, as an attempt to know the capability in modeling their crystal structure throughout SimulaTEM software and

16

Gatan microscope post-processing tools. So, on the basis of the present results, the following conclusions can be drawn:

1) Thermodynamic predictions carried out using FactSage$^®$ at intermediate temperature range of 800-900 °C have shown good agreement with found VC and TiC precipitated particles in the experimental TWIP steels.

2) Characteristic morphologies were identified, depending directly in their crystallographic orientation, e.g. hexagonal-type in the case of VC particles and rectangle-type in the case of TiC ones. Large and small particles were measured in both TWIP steel. Particle sizes ranged 10 to 190 nm in both TWIP steels.

3) NaCl-type crystal structure in both VC and TiC precipitates was observed.

4) HRTEM images treatment by Gatan post-processing tools and SimulaTEM software allowed modelling crystal structure, measuring the interplanar spacing and identify each type of precipitate, VC for V-containing TWIP steel and TiC for Ti-containing TWIP steel.

5) HRTEM image processing employing carbon extraction replicas is helpful in identifying and measuring crystallographic features of precipitates in microalloyed TWIP steels.

**References:**

[1]    D. Barbier, N. Gey, S. Allain, N. Bozzolo, M. Humbert, *Mater. Sci. Eng. A* **2009**, *500*, 196.

[2]    S. Kang, J.G. Jung, Y.K. Lee, *Mater. Trans.* **2012**, *53*, 2187.

[3]    F. Reyes-Calderón, I. Mejía, A. Boulaajaj, J.M. Cabrera, *Mater. Sci. Eng. A* **2013**, *560*, 552.

[4]    A.E. Salas-Reyes, I. Mejía, A. Bedolla-Jacuinde, A. Boulaajaj, J. Calvo, J.M. Cabrera, *Mater. Sci. Eng. A* **2014**, *611*, 77.

[5]    L. Llanos, B. Pereda, B. Lopez, J.M. Rodriguez-Ibabe, *Mater. Sci. Eng. A* **2016**, *651*, 358.

[6]    Research Found for Coal and Steel, Precipitation in high manganese steels, European Commission, **2014**, p. 11, 138.

[7]    D. Acevedo-Reyes, M. Pérez, C. Verdu, A. Bogner, T. Epicier, *J. Microsc.* **2008**, *232*, 112.

[8]    J.H. Jang, C.H. Lee, Y.U. Heo, D.W. Suh, *Acta Mater.* **2012**, *60*, 208.

[9]    A. Teresiak, H. Kubsch, Nanostruct. Mater. **1995**, *6*, 671.

[10]   J. Bobynko, A.J. Craven, D. McGrouther, I. MacLaren, G. Paul, *J. Phys.: Conf. Ser.* **2014**, *522*, 012031.

[11]   J. Bobynko, I. MacLaren, A.J. Craven, Ultramicroscopy **2015**, *149*, 9.

[12]   FSstel Database, in: ⟨http://www.factsage.com⟩.

[13]   C.W. Bale, E. Bélisle, P. Chartrand, S.A. Degterov, G. Eriksson, K. Hack, I.H. Jung, Y.B. Kang, J. Melancon, A.D. Pelton, C. Robelin, S. Petersen, *Calphad* **2009**, *33*, 295.

[14]   A. Gómez, L. Beltrán del Río, *Rev. LatinAm. Metal. Mater.* **2001**, *21*, 46.

[15]   T.N. Baker, *Mater. Sci. Technol.* **2009**, *25*, 1083.

[16]  E. Rudy, F. Benesovsky, *Pulvermetall.* **1962**, *10*, 42.

[17]  P. Villars, *Pearson's Handbook-ASM International*, Materials Park, OH, **1997**.

[18]  H.W. Yen, M. Huang, C.P. Scott, J.R. Yang, *Scr. Mater.* **2012**, *66*, 1018.

[19]  G. Brauer, W.D. Schnell, *J. Less Common Met.* **1964**, *7*, 23.

[20]  E.T. Turkdogan, *Iron Steelmaker* **1989**, *3*, 61.

[21]  H.A. Wriedt, H. Hu, *Chemical metallurgy*, (Ed. N.A. Gokcen), Warrendale, PA, The Metallurgical Society of AIME, **1981**, pp. 71–194.

[22]  T. Wada, H. Wada, H. Elliott, J. Chipman, *J. Metall. Trans.* **1972**, *3*, 2865.

[23]  N.A. Savostyanova, L.A. Shvartsman, *Phys. Met. Metallogr.* **1960**, *9*, 35.

[24]  T. Gladman, *The physical metallurgy of microalloyed steels*, The Institute of Materials, UK, **1997**, pp. 298-303.

[25]  K. Narita, *Trans. Iron & Steel Inst. of Japan* **1975**, *15*, 145.

[26]  R.H. Ogden, R.I. Jaffee, F.C. Holden, *Trans. AIME, JOM.* **1955**, *7*, 73.

[27]  C.R. Hubbard, *Standard X-ray diffraction powder patterns - Section 18*, National Bureau of Standards, International Centre for Diffraction Data, USA, **1981**, p. 73.

[28]  M. von Schwarz, O. Summa, *Elektrochem.* **1932**, *38*, 743.

[29]  Y. Lv, W. Gao, *Modern Physics Letters B* **2016**, *30*, 1650334.

[30]  V.S. Sinel'nikova, T.I. Shtukaturova, L.V. Strashinskaya, T.I. Shaposhnikova, G.S. Burkhanov, V.A. Kuz'mishchev, *Structure and properties of fused single-crystal titanium carbide,* Plenum Publishing Corporation, **1982**, pp. 560-563.

[31]  H.Y. Yen, C.Y. Chen, T.Y. Wang, C.Y. Huang, J.R. Yang, *Mater. Sci. Technol.* **2010**, *26*, 421.

Manuscript srin.201900098R1-TEM characterization and high-resolution modelling of second-phase particles of V and Ti containing TWIP steel under uniaxial hot-tensile condition.

**Table of Contents (TOC) text and figure:**
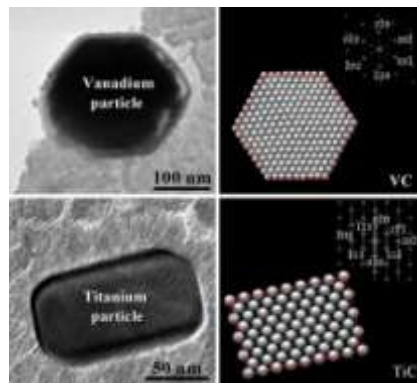


The use of V and Ti microalloying elements in forming carbide particles is very important in high-Mn TWIP steels because their influence on mechanical behavior. In this study, a predictive model was proposed by coupling a HRTEM image with SimulaTEM/Gatan post-processing tools. Results were compared with particles extracted via carbon replica technique. Thus, image treatment allowed identifying particle crystallographic features.